3 Biotech (2021) 11:160
https://doi.org/10.1007/s13205-020-02567-w

ORIGINAL ARTICLE

Optimization and evaluation of ciprofloxacin-loaded collagen/chitosan scaffolds for skin tissue engineering

Satyavrat Tripathi[1] · Bhisham Narayan Singh[1] · Divakar Singh[1] · Gaurav kumar[2] · Pradeep Srivastava[1]

Received: 7 June 2020 / Accepted: 24 November 2020 / Published online: 7 March 2021

Abstract

A novel ciprofloxacin-loaded collagen–chitosan scaffold was developed for the treatment of wound using freeze drying method. The average pore size and porosity of developed scaffold was found to be around 125 µm and 91 ± 0.56%. Moreover, swelling, degradation and mechanical tests profile supported the suitability of scaffold for wound healing process. The scaffold has high degree of hemocompatibility towards the blood and promotes the growth, migration and proliferation of fibroblast. The developed scaffold exhibits antibacterial properties and was found to be efficient against the Gram-negative (*E.coli*) and Gram-positive (*Staphylococcus aureus*) bacteria hence can be used for wound healing applications. In vivo study demonstrated that the scaffold not only escalated the tissue regeneration time but also accelerated the wound healing process compared to control. The histological studies revealed better granulation, vascularization, and remodeling of extracellular matrix along with regeneration of epidermal and dermal layer of skin. Overall, the obtained results suggested that the developed skin tissue constructs possess the enormous potential for tissue regeneration and might be a suitable biomaterial for skin tissue engineering applications.

Keywords Scaffold · Collagen · Chitosan · Would healing · Ciprofloxacin

Introduction

Skin is the largest human organ that reaches 10% of the total body mass and plays prominent role in first line of barrier between outer environment and body, sensory detection, thermoregulation, fluid homeostasis and immune surveillance (Boucard et al. 2007; Metcalfe and Ferguson 2007). Wound is an open injury that disrupts the structure and anatomy that ultimately meddles with the fidelity and integrity of the skin. Wound healing is a very complex process of repairing and replenishing the damaged parts of the skin and restores its normal functions. Under any unfortunate conditions including accidents, burning and the disease progression such as diabetes the excessive loss of the skin takes place. Skin tissue possess natural tendency of healing to maintain the physical and chemical integrity of skin. Process of wound healing is a complex and dynamic cascade of events initiated with occurrence of injury that involve coordinated cell activation, cell division, chemotactic cell migration, and differentiation of various cell types. The sequence of events begins at the moment of injury, which involves platelet aggregation, blood clotting, cell migration and tissue formation and tissue remodeling (Enoch and Leaper 2008).

In case of any unfortunate conditions such as extreme burn, occurrence of scar or extreme large size of skin defect/damages needs development of various skin substitutes to accelerate the wound healing process and overcome the limitations of natural wound healing process. Skin substitutes are the heterogeneous class of wound healing substance that

✉ Pradeep Srivastava
pksrivastava.bce@itbhu.ac.in

Satyavrat Tripathi
Satyavrat4@gmail.com

Bhisham Narayan Singh
Bhisham6@gmail.com

Divakar Singh
singhdivakar686@gmail.com

Gaurav kumar
Gaurav.rs.bme14@itbhu.ac.in

[1] School of Biochemical Engineering, Indian Institute of Technology (Banaras Hindu University), Varanasi 221005, India

[2] School of Biomedical Engineering, Indian Institute of Technology (Banaras Hindu University), Varanasi 221005, India

assist or aid in epidermal or dermal wound healing. The most common skin substitutes such as xenografts, allograft and autografts are commonly considered for the treatment of wound healing. However, many limitations such as antigenicity, scar formation and poor tissue integration are associated with these developed constructs (Shevchenko et al. 2010). A porous wound healing dressing material provides three-dimensional matrix, which promotes cell adhesion, migration and proliferation, absorbs wound exudates, provide protection against the microbes, maintain moisture and allow the gaseous exchange to environment (Mayet et al. 2014; Jayakumar et al. 2011). Numerous natural polymers such as chitosan, collagen, gelatin, hyaluronic acid, silk, etc. have a great potential to be used in tissue engineering to develop novel wound healing dressing skin substitutes (Kumari et al. 2019). Moreover, natural biopolymers are, biocompatible, biodegradable and provides biomimetic extracellular matrix for tissue regeneration (Francesko and Tzanov 2010; Sionkowska 2011).

Collagen is the most abundant protein in animal tissues and accounts for 70–80% of the dry weight of the dermis. Collagen is the unique, triple helix protein molecule, which forms the major part of the extracellular dermal matrix (ECM). The principal function of collagen is to act as a scaffold in connective tissue. It also offers low immunogenicity, porous structure, good permeability, biocompatibility and biodegradability (Hopkinson 1992a, b). In spite of all these advantages, the poor mechanical strength of its constructs limits its applications in tissue engineering (Dong and Lv 2016; Ma et al. 2003). Therefore, to enhance the mechanical strength of the construct it has to mix with other natural or synthetic polymers (Dong and Lv 2016). Synthetic polymers as Poly(lactide–co–glycolide) (PLGA), Poly(–caprolactone) (PCL), Poly(3–hydroxy butyrate–co–3– (Dong and Lv 2016) hydroxyvalerate) (PHBV), Polyurethane (PU), Poly(L—lactide) (PLLA), Poly(L–lactic acid)–co–poly(–caprolactone) (PLCL) have been used for tissue engineering but synthetic polymers share serious disadvantages like acid degradation products, slow degradation rate, high Hydrophobicity, less cytocompatibility, and mechanical stiffness (Kumbar et al. 2008; Chong et al. 2007; Heo et al. 2013; Jin et al. 2011; Kim et al. 2009; Nguyen et al. 2013; Venugopal and Ramakrishna 2005).Therefore, to overcome the limitations of synthetic polymers, it is mixed with chitosan, that increases the mechanical stability and promotes the slow degradation of scaffold (Dong and Lv 2016; Tangsadthakun et al. 2017).

The deacetylated derivatives of chitin, reported as chitosan, have wide application in wound management, because it has capacity to deliver the loaded drug in tissue surface (Mahato et al. 2019). Moreover, chitosan is hypoallergenic, antibacterial, biocompatible, and biodegradable with high mechanical strength and facilitate quick blood coagulation at the site of injury (Suzuki et al. 1998; Chen et al. 2017; Susanto et al. 2019; Jia et al. 2011). Wound infection is the major concern in wound healing. Wound infection by bacterial agent leads to the impairment of the wound healing process which leads to the delay in the healing process (Guo and DiPietro 2010).

Ciprofloxacin HCl, a fluoroquinolone antibiotic, is effective against both Gram-positive and -negative bacteria that cause wound infection, is one of the most widely used antibiotics in wound healing as it has very low minimum inhibitory concentration against the bacteria (Unnithan et al. 2012; Yu et al. 2006). Thereby, ciprofloxacin might be suitable to generate drug-loaded tissue construct for skin tissue engineering application. Therefore, the aim of present study is to optimize, fabricate, characterize and evaluate ciprofloxacin-loaded collagen–chitosan scaffold (COL/CHI/CPX) using freeze drying process. Developed matrix exhibit enhanced mechanical strength, structural stability and integrity in both wet and dry conditions, which is also a major limitation associated with chitosan based matrix for wound healing. We used dual cross-linking system of EDC/NHS and glutaraldehyde to enhance scaffold mechanical properties. Furthermore, ideally wound healing matrix need to maintain optimal physico-chemical and mechanical properties and should release antibiotics to overcome the infections at the wound site. In the present study, first time we reported development of chitosan/collagen based matrix loaded with ciprofloxacin, which was observed to be a potent antibiotic against various Gram-positive and Gram-negative bacteria, also reported to be potential antibiotic against most common bacterial infection of *Staphylococcus aureus* and *E.coli* at wound site. Moreover, developed scaffold was characterized for its physico-chemical properties and evaluated for various biological properties through in vitro and in vivo study.

Materials and methods

Chitosan (Medium molecular weight), Collagen peptide (bovine origin). Ciprofloxacin hydrochloride, Lysozyme, 1-ethyl-3-(3-dimethylaminopropyl) carbodiimide hydrochloride (EDC), N-hydroxysuccinimide (NHS), and Trypsin (0.25%) were purchased from Himedia, India. Paraformaldehyde, Triton X-100, 3-(4,5-dimethylthiazol-2-yl)-2,5-diphenyl tetrazolium bromide (MTT), Ammonium hydroxide, Glacial acetic acid (100%), Ethanol, Dimethyl sulfoxide (DMSO), Nitric acid, 4,6-diamidino-2-phenyindole (DAPI), and Hematoxylin–Eosin staining solution were purchased from Sigma Aldrich, (St.Louis, USA). Dulbecco's Modified Eagle Medium (DMEM), Fetal bovine serum (FBS), and Antibiotic–Antimycotic solution were purchased from Gibco, (USA). Phosphate buffer solution (PBS) was purchased from Invitrogen, USA, and Cyclohexane (Merk Millipore). All the

remaining chemicals were supplid by local firms and were of highest purity grade and double distilled water (DDW) was used throughout the experiment.

Porous biopolymeric ciprofloxacin-loaded collagen/chitosan scaffold (COL/CHI/CPX) was prepared through freeze drying process. Collagen (1.5 w/v) and chitosan (1.0% w/v, 1.5% w/v and 2.0 w/v %) solution were prepared in 1% glacial acetic acid solution. Ciprofloxacin was added in during the preparation of collagen/chitosan blend solutions to obtain antibiotic concentration 2 mg/ml. The collagen/chitosan (COL/CH) scaffolds were fabricated through blending of COL/CH solutions in different concentration as mentioned in Table 1.

After appropriate mixing of COL/CH solution in above-mentioned concentrations the obtained solutions were placed at − 20 °C for overnight. After freezing, the frozen sample was subjected to lyophilisation for 24 h using lyophilizer (Lab Corno USA). Dual cross-linking was performed to provide the better mechanical strength to scaffold. Glutaraldehyde as a cross-linking agent provides good mechanical strength but makes the scaffold brittle. Besides glutaraldehyde, EDC/NHC was also recruited as a cross-linking agent but it also failed to maintain the structural integrity of scaffold. Therefore, dual cross-liking has been employed to attain the scaffold having structural integrity and fidelity. Using varied concentrations of glutaraldehyde and EDC/NHC at different time points, the optimum concentration was achieved to attain the best scaffold. In the first step, scaffold was cross-linked using, 1-ethyl-3-(3-dimethylaminopropyl) carbodiimide hydrochloride (EDC) and N-hydroxysuccinimide (NHS) for 12 h. The cross-linking solution was prepared as 3% EDC/NHS [2:1 (w/w] in [(95:5 v/v (ethanol: water)]. After 12 h of treatment, scaffold was transferred in a second cross-linking solution containing 1% glutaraldehyde in 50:50 v/v (ethanol: water) for 12 h. After cross-linking, the obtained scaffolds were washed three times with double distilled water. The cross-linked scaffold was freezed overnight and then freeze-dried using lyophilizer (Lab Corno USA) for 24 h.

Table 1 Details of scaffold preparation at varied concentration of collagen and chitosan solutions

	Collagen (%)	Chitosan (%)	Result
Scaffold-1 (SC-1)	1.5	1.0	Scaffold prepared
Scaffold-2 (SC-2)	1.5	1.5	Scaffold prepared
Scaffold-3 (SC-3)	1.5	2.0	Scaffold prepared

Characterization

Morphological and physical characterization

The developed porous scaffold was characterized for its morphology, pore size, and its distribution using the Scanning electron Microscope (SEM). Each scaffold was cut in to small pieces and coated with gold using a gold sputter and finally, scaffold samples were then studied with a Zeiss Evo-18, SEM, Germany at 10 kV. The average pore size was obtained by measuring the maximum and minimum diameter in the image section of at least 30 pores chosen randomly in each SEM images using ImageJ software (NIH, USA).

Porosity of the developed scaffold was measured be using liquid displacement method. Scaffold samples were submersed in cyclohexane for 1 h allowing all pore of scaffold to be filled with liquid. According to the liquid displacement theory, the volume of a scaffold immersed in the fluid is equal to the volume of the displaced fluid, and we can calculate the porosity from the following equation (Maquet et al. 2004; Mabrouk et al. 2014; Singh and Pramanik 2018):

$$\text{Porosity} = \frac{W_1 - W_3}{W_2 - W_3} \times 100,$$

where (W_1) is the weight of the scaffold before immersion, (W_2) is the weight of the scaffold after immersion and (W_3) is the weight after drying. All the experiments were conducted in triplicate ($n = 3$).

Swelling and degradation behavior of scaffold

The swelling percentage was estimated by the conventional gravimetric method. Swelling behavior of scaffold was evaluated using pieces of scaffold (15 mm × 15 mm × 5 mm, length × weight × height) ($n = 3$). Scaffold samples were dipped into a beaker containing phosphate buffer saline (PBS) of pH 7.4 at a temperature of 37 °C. Thereafter, soaked scaffolds were taken out from PBS, wiped with filter paper and weighed at the interval of 6 h for the period of 24 h. Swelling percentages was calculated as:

$$\text{Swelling percentage} = \frac{W_t - W_0}{W_0} \times 100,$$

where W_0 is the initial weight of the scaffold, W_t is the weight of scaffold after different time intervals (Ma et al. 2003).

Contact angle analysis was carried out to find out the wettability of the developed scaffold. The contact angle of developed scaffolds were measured at room temperature (25 ± 1 °C) using sessile drop method by placing 10 µl of distilled water over the surface of develop scaffolds and

angle was measured using Image J. software. Contact angle was measured by taking six reading at different parts of the scaffold and value was averaged (Liu et al. 2017).

An ideal scaffold should have a proper degradation behavior to match with the regenerating process of the damaged tissue or organ. The degradation behavior of scaffolds was evaluated using lysozyme degradation method. Briefly, the biodegradation of scaffold was evaluated by measuring the change in weight of the scaffold at different time intervals in phosphate buffer saline (PBS) at pH 7.4. Lysozyme based solution was prepared with the concentration of 1.4 µg/ml or 120 units/ml. Then, the scaffolds of known weight were transferred in the enzymes solution and weight of scaffold was recorded after preferred time intervals. Lysozyme solution was changed after every 3 days and biodegradation (D) was calculated using the following equation:

$$D(\%) = \frac{W_0 - W_t}{W_t} \times 100,$$

where W_0 is the dry weight of scaffold before degradation and W_t is the dry weight of scaffold after degradation (Wang and Tsai 2013; Arakawa et al. 2017).

FTIR analysis

Fourier-transform infrared spectroscopy (FTIR) is a quantitative analytical technique extensively used to identify inorganic, organic and polymeric materials. In present study, FTIR was performed for the analysis of chemical interaction between collagen and chitosan in blend. FTIR of scaffolds were performed at done in the range of 4000–600 cm^{-1} by KBr pellet method (FTIR-8400S, Shimadzu, Japan).

Mechanical study

The mechanical properties of the scaffolds were determined in terms of tensile strength using texture analyzer (CT3Brookfield, Germany). The scaffolds were cut into quadrangles of 5 cm × 1 cm, and the thickness of the scaffold was maintained around 3 mm, which was measured by vernier caliper (Mitutoyo 8" Vernier Caliper Model 502-231). Tensile strength of scaffold was measured in both dry and wet condition. The test speed was maintained around 0.05 mm/s and the gripping distance was 40 mm. All the experiments were performed in triplicate ($n = 3$).

Thermal property study

The thermodynamic property of the scaffolds was analyzed using Differential Scanning Calorimeter (DSC Q200) under N_2 atmosphere at a heating rate of 10 °C/min with the sample size of 5 mg. Pyrolytic pattern of the samples was obtained using a Thermo Gravimetric Analyzer (TGA-Q50) under N_2 atmosphere at a heating rate of 10 °C/min with a sample size of 5 mg.

Antimicrobial study

The developed scaffold was evaluated for antimicrobial properties against *E. coli* (Gram negative) and *S. aureus* (Gram positive) for the antibacterial test. These bacteria were cultured in sterilized Lysogeny broth medium and then incubated overnight at 37 °C in the incubator (Tallian et al.). The antibacterial activity of SC-3 was investigated by measuring the zone of inhibition. Scaffolds were cut into circular discs (1.0 cm in diameter) and antibacterial test was performed in test and control samples. In control, scaffold without antibiotics was used and bacteria were cultured in agar plates using spread platting method inoculated with 1 ml of a bacterial suspension containing around 100 cfu/ml. The scaffold was placed at the center of the agar plate and agar plates were incubated at the 37 °C (Lim and Sultana 2016). All the test was performed in triplicate ($n = 3$).

Hemocompatibility study

Hemocompatibility test was performed to measure the extent of haemolysis of RBCs in presence of the developed scaffolds. It was performed as per ASTM protocol. Tests were performed using goat blood, which was collected in the presence of Trisodium citrate (TSC) (3.8 gm in 100 ml of blood). Citrate blood was diluted with normal saline in 8:10 ratio using 0.5 ml of diluted blood and 9.5 ml normal saline in a falcon tube. Thereafter, scaffold of size 10 mm × 10 mm × 3 mm (length breath and height, respectively) was inserted inside the falcon tube at 37 °C at 50 rpm. Positive and negative controls were taken into consideration. In positive control, 0.5 ml of diluted blood is mix with 0.5 ml of of 0.01 N HCl and volume is made 10 ml with normal saline. In negative control, 0.5 ml of diluted blood was mixed with normal saline to make volume 10 ml. All the samples were centrifuged and the absorbance of the supernatant was measured at 545 nm to calculate the percent of haemolysis as follows:

$$\%\text{Hemolysis} = \frac{\text{OD}_{\text{test}} - \text{OD}_{\text{negative}}}{\text{OD}_{\text{positive}} - \text{OD}_{\text{negative}}} \times 100.$$

If % haemolysis is more than 20% then non-hemocompatible.

If less than 5%, then highly hemocompatible.

If 5–10%, then hemocompatible (Dey and Pal 2009; Mallick et al. 2018).

In vitro drug release

Drug release study of ciprofloxacin form collagen–chitosan scaffold was carried out using an automated Franz diffusion cell apparatus (Microette Plus™; Hanson Research, Chatsworth, USA) with the basket method at 100 rpm. A volume of 900 mL phosphate buffer pH 7.4 equilibrated at 37 °C was utilized as dissolution fluid. The prepared scaffolds were placed between the donor and receptor compartments. Isotonic phosphate buffered saline (pH 7.4) was used as a release medium in the receptor chamber and was maintained at 37 °C with stirring rate of 100 rpm. Aliquot samples (2 ml) were withdrawn by the auto sampler and appropriately diluted to analyze for drug content spectrophotometrically at 540 nm (Shimadzu, UV-1800 spectrophotometer, Japan). A cumulative percentage of release of ciprofloxacin form scaffold was in vitro examined for a period of 20 h, and a relationship between the percentage drug release and releasing time was plotted (Mahmoud and Salama 2016).

Cell attachment and proliferation study

Fibroblast cells were isolated from the rat skin, using collagenase and trypsin as described by the method in literature (Seluanov et al. 2010). Isolated fibroblasts cells were cultured in DMEM-L glucose, supplemented with 10% FBS, 0.1% antibiotic–antimycotic solution and incubated at 37 °C with 95% humidity in 5% CO_2 incubator in T-25 cell culture flask until the 70–80% confluency was attained. At confluence, cells were harvested and subculture in the same medium. Culture media was changed in every 3 days. Scaffold of defined dimension (10 mm × 10 mm × 2 mm) (length × breadth × thickness) were taken and sterilized using 70% ethanol and UV sterilization. Scaffolds were left into culture media overnight to check for any infection/contamination. Fibroblast cells were separated from flask using 0.25% trypsin. Cells were centrifuged at 300 g for 10 min and cell counting was done using hemocytometer. The scaffolds were placed in the 16-well plate and fibroblast cells were seeded in cell density of 1×10^5 per ml for predominated period. The culture plate was placed inside the incubator and media was changed in every 72 h. All the experiment were run in triplicate ($n = 3$) (Udhayakumar et al. 2017).

The fibroblast morphology and attachment over cultured scaffolds namely SC-1, SC-2 and SC-3 were studied for the period of 5, 10, and 15 days using SEM and florescence microscopy. In brief, the scaffolds were washed with PBS thrice and then fixed with 2.5% glutaraldehyde. The scaffolds were further serially dehydrated using ascending grade of ethanol (10, 20, 30, 50, 70, and 100%). The dehydrated scaffolds were coated with the gold particle using gold sputter coater and morphology of cells over the scaffold was observed using SEM. The proliferation of cells in scaffolds was studied using fluorescent stain using DAPI and images were collected using fluorescence microscope.

DNA content estimation

Proliferation of fibroblasts over developed scaffolds was evaluated through total DNA content assay. The amount of DNA associated with the fibroblast over the scaffolds was measured with a PicoGreen Quantification Kit (Molecular Probes). Briefly, the cell-cultured scaffolds were taken out at different time intervals (5, 10 and 15 days), washed thrice with PBS and treated with 1.0 ml of cell lysis buffer for 30 min. Lysis buffer contains 10 mM Tris (pH 8), 1 mM EDTA, and 0.2% (v/v) Triton X-100. After cell lysis, the samples were centrifuged at 300 g for 10 min and supernatant was collected while pellet was discarded. 100 µl of sample was mixed with 100 µl of DNA-binding fluorescent dye solution. Intensity was measured through a spectrofluorometer at an excitation wavelength of 480 nm and an emission wavelength of 530 nm. Standard curve was prepared using lambda DNA. All the experiments were performed in triplicate ($n = 3$) (Wu et al. 2015).

MTT assay

Metabolic activity of cells over the developed scaffolds was determined using the MTT (3- dimethylthiazol-2,5-diphenyltetrazolium bromide) based colorimetric assay as previously described in Intini et al. (2018); Mitra et al. (2018); Khandelwal et al. (2019); Singh et al. (2020). Fibroblast were cultured over the scaffold up to 15 days and metabolic activity was examined on 5th, 10th and 15th day after adding MTT (10 µl of a 1 mg/ml stock) in the wells of culture plate followed by incubation at 37 °C for 3 h under CO_2. Mitochondrial enzymes of viable cells reduced the yellow-colored MTT into purple-colored formazan crystals; which were dissolved in 200 µl of DMSO for 15 min. Finally, absorbance of the solubilized formazan derivative was recorded at the wavelength of 540 nm using the microplate reader.

In vivo wound healing

Based on the physical, chemical, and mechanical characterization of all scaffolds SC-2 was selected for wound healing experiment on rat animal model. An in vivo study was conducted according to institurional guideline and strictly followed the norms of the committee for the purpose of supervision and control on experiments on animals (CPSCEA), Government of India. Ethical approval number is DEAN/2017/CAEA/99. Skin flap model was considered for wound healing study and the experiment was conducted on 2-month-old rat having weight 250–300 g. The animals

were kept in environmentally controlled rooms (25° ± 2 °C, humidity 50 ± 5%, 12 h light and dark cycle) and kept in cages individually supplied with food and water ad libitum. Wound in rat was created after anesthetizing them using intraperitoneal injection of 50 mg/kg ketamine and 5 mg/kg xylazine. The full thickness of the dermis, with dimension of 1.5 cm × 1.5 cm, was removed from the back of rat. Six rats were randomly selected into two group having three rat in each group. Group one was selected as control, which was devoid of scaffold at the site of wound. Whereas test group consist of COL/CHI/CPX scaffold placed at the wound. Wound was covered with dressing bandages and the dressing materials were changed at every 4 days. Wound area was quantified by taking photograph at different time intervals until the wound healing process completed. The degree of wound healing was determined by measuring the area of the wound with respect to a ruler by means of Image J software. Wound healing rate was calculated using the formula available in the literature (Karri et al. 2016):

$$\text{Wound healing rate} = \frac{A_0 - A_t}{A_0} \times 100,$$

where A_0 initial area of wound, A_t area of wound remain after time (t).

Histopathological study

Samples were excised from the area of the wound at different time periods of 5th, 10th, 15th day and immediately fixed in PBS-buffered 4% paraformaldehyde at pH 7.4. Further samples were dehydrated in ascending grades of ethanol, cleared in xylene and embedded in paraffin wax. The samples were sectioned at 4 µm using the microtome and mounted on poly-L-lysine coated slides. The sections were deparaffinized in xylene and rehydrated in descending grades of ethanol followed by Hematoxylin–Eosin staining and observed under an inverted routine microscope (Hollister 2005; Sun et al. 2015) (TS100, Nikon, Eclipse, Japan).

Result and discussion

Morphological and physical characterization

The morphology of the prepared scaffolds is shown in Fig. 1. SEM image of prepared scaffold has shown a vivid range of interconnected micro and macropores. Coexistence of macro- and microporous structure is suitable not only for cell growth but also for the exchange of nutrients and removal of the waste (Wong et al. 2008). Pore size of the developed scaffolds ranges from 48 to 169 µm. but average pore size of scaffolds was calculated using Image J software were found to be around ~ 71 µm, ~ 125 µm and ~ 142 µm for SC-1, SC-2 and SC-3, respectively. Pores are long and interconnected that are essential for cell nutrition, proliferation migration for tissue vascularization for new tissue formation (Loh and Choong 2013). As the chitosan, percentage increases the thickness of the pore wall increases and porosity decreases. Porosity is important physical parameter of need to keep in mind during the designing of the scaffold. High porosity of scaffold is necessary as it enable the effective release of biofactors, antibiotics, cell attachment and cell migration; however, the mechanical strength is often compromised in highly porous structure therefore a balance between the porosity and mechanical strength need to achieve (Hollister

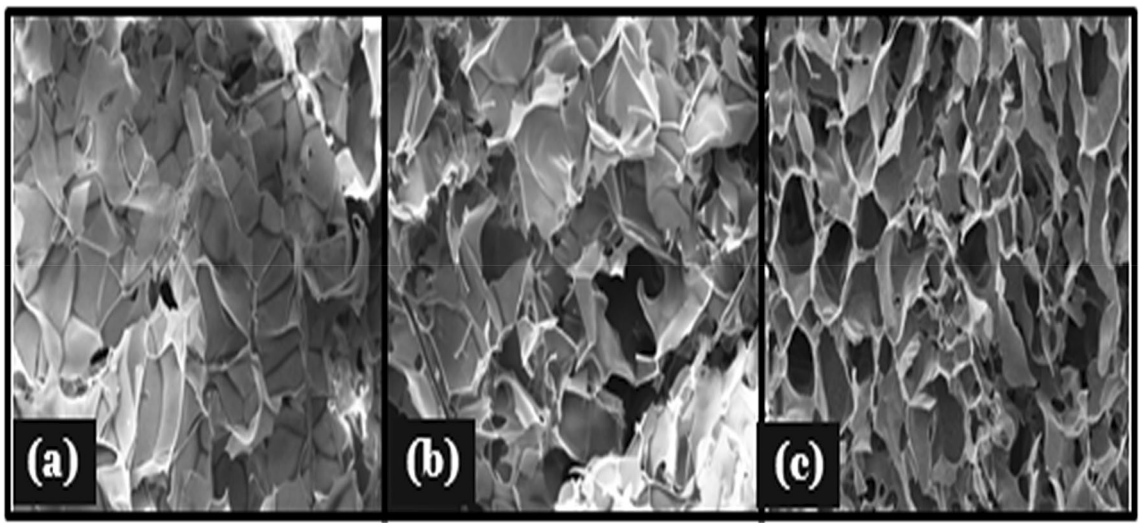

Fig. 1 SEM images of developed scaffold SC-1 (**a**), SC-2 (**b**), and SC-3 (**c**), respectively, showing morphology and distribution of pores

2005). Prepared scaffold shows highly porous structure having the porosity of scaffold above 90% for the entire set of fabricated scaffolds. Porosity of scaffolds is SC-1, SC-2 and SC-3 is 93 ± 0.25%, 91 ± 0.56% and 87 ± 0.25%, respectively (Fig. 1).

Swelling and degradation behavior of scaffold

Percentages of swelling of COL/CHI/CPX based scaffolds are shown in Fig. 2. Scaffold should maintain its structural integrity under wet condition to support cell growth, migration and proliferation. Since collagen and chitosan both are highly hydrophilic polymer and thereby scaffolds were cross-linked to improvise the structural integrity and stability of the scaffold (Ahmadi et al. 2015). Furthermore, cross-linking results in reduction of free hydrophilic group and allows scaffold to maintain its three-dimensional structure. The measured contact angle of the composites is shown in Fig. 2c. The hydrophilic or hydrophobic property of scaffold surface is an important factor that affects the cell affinity towards the scaffold. In most cases, the capacity for cell attachment and proliferation on a hydrophilic surface is better than on a hydrophobic surface. The contact angles for SC-1, SC-2, and SC-3 was found to be 74 ± 0.42°, 63 ± 0.54°, and 59 ± 0.24°, respectively. It was found that the contact angle of scaffold decreased with increased chitosan amount which might be due to higher chitosan in scaffold. It was observed that the contact angle of scaffold decreases with increasing chitosan content and thus scaffold with higher content of chitosan shows lower contact angle value indicating its higher hydrophilicity. Also, swelling behavior of scaffold was observed to be in accordance with contact angle or hydrophilicity of the matrix. It has been observed that cross-linked matrix of chitosan based scaffold shows controlled swelling in the range of 40–300% as compared of previously reported chitosan based matrix with higher degree of swelling behavior in the range of 500% (Chhabra et al. 2016; Mahmoud and Salama 2016; Tylingo et al. 2016). Thus, the developed scaffold shows controlled swelling behavior and might be suitable for the skin tissue regeneration.

Biodegradation is an important parameter taken into consideration while designing of scaffold for tissue regeneration. Degradation of scaffold should match at least partially with the regeneration of tissue at the implant site. Lysozyme is exclusively present in human blood serum at high concentration at wound site produced by human immune system as direct reflection of host immune response (Shah et al. 2019; Tallian et al. 2019; Torsteinsdóttir et al. 1999). Therefore, lysozyme was used for biodegradation study. Lysozyme hydrolyzes the β(1–4) glycosidic bond between *N*-acetyl-glucosamine and glucosamine in chitosan (Kim et al. 2018). Moreover, from the graph, it can be observed that SC-1 has least rate of degradation in comparison to SC-2 and SC-3. Also, pH of solution during the degradation remains in the range of 6.8–7.4. SC-3 shows very high rate of degradation in comparison with SC-2 and SC-1 which might be due the presence of the chitosan in higher amount and presence of beta-glycosidic bond in the complex scaffold. These higher concentrations of chitosan leads to high rate of degradation in SC-2 and SC-3 compare to SC-1 (Fig. 2).

FTIR analysis

Fourier-transform infrared spectroscopy (FTIR) is used to illustrate their functional chemical group characteristics. FTIR spectrum shows the mix characteristics of collagen and chitosan as reported earlier by various investigators (Fig. 3). In cross-linking process, various chemical groups react together to form a stable cross-linked structure.

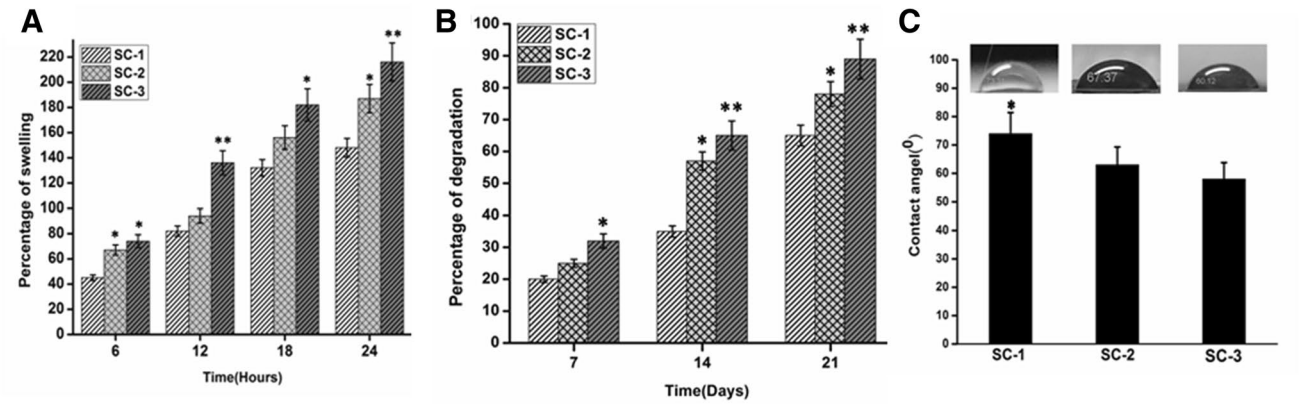

Fig. 2 **a** Depicting the percentage of swelling of developed scaffolds at different time intervals. **b** Representing the percentage of degradation of developed scaffolds at different time intervals. **c** Measurement of contact angle of developed scaffolds. Data are expressed in terms of mean ± SEM ($n = 3$), ($^{*}p < 0.01$), ($^{**}p < 0.001$)

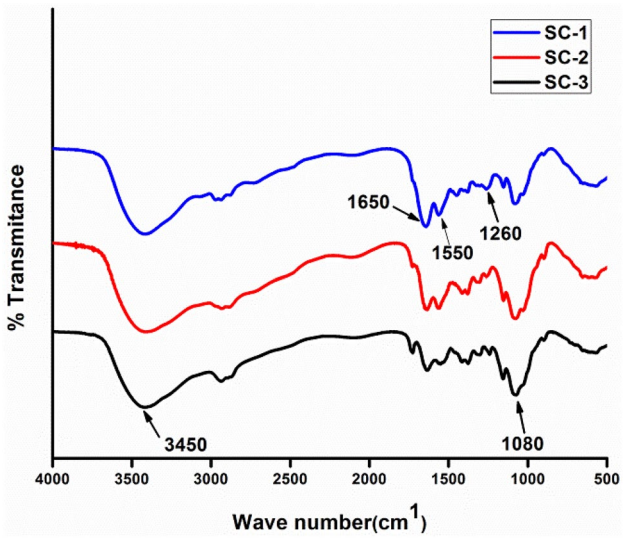

Fig. 3 FTIR Spectrum of collagen–chitosan scaffolds depicting the characteristic peaks of scaffolds

Glutaraldehyde reacts with the amine or hydroxyl functional group of proteins and polymers, respectively, through a Schiff-base reaction and connects the biopolymeric chains via intra- or intermolecular interactions (Chajra et al. 2008). EDC/NHC activates carboxyl groups and forms an amine reactive O-acylisourea intermediate that spontaneously reacts with primary amines to form an amide bond and isourea as a by-product. From the FTIR spectrum, it can be inferred that characteristic peak of collagen and chitosan are present in the scaffolds. Characteristic peak of collagen can be seen in 1650 cm^{-1} which represents the amide I bands (1659 cm^{-1}) originated from C = O stretching vibrations coupled to N–H bending vibrations, 1560 cm^{-1} that attributed to the amide II band arise from the N–H bending vibrations coupled to C–N stretching vibrations and 1260 cm^{-1} which correspond to represented the combination peaks between N–H deformation and C–N stretching vibrations (Ungureanu et al. 2015). 1080 cm^{-1} and 3450 cm^{-1} are characteristic peaks of chitosan represent glycosidic bond and –OH group, respectively (Fernandes et al. 2011; Ungureanu et al. 2015; Andonegi et al. 2020). Characteristic intense peak (1080 cm^{-1}) of chitosan, such as glycosidic linkages, appeared more clearly when the composition of chitosan was increased. For example, the intensity of amide I peak at 1650 cm^{-1} decreases gradually with increase in the proportion of chitosan (Tangsadthakun et al. 2017). Furthermore, the wave number difference between amide I and amide II bands was lower than 100^{-1} which indicated that the triple helix structure of collagen was maintained upon mixing of collagen with chitosan (Sizeland et al. 2018).

The difference in the relative intensity between FTIR bands suggested interactions between collagen and chitosan, probably by hydrogen bonding among carboxyl, amino, and hydroxyl groups present in the components of the scaffold forming formulation (Andonegi et al. 2020) (Fig. 3).

Mechanical study

The tensile strength of scaffolds was measured in dry and wet condition. Tensile strength of SC-2 was found to be 7.12 MPa in comparison to SC-1 and SC-3 which having tensile strength of 6.70 MPa and 2.8 MPa, respectively, at dry condition (Fig. 4). The tensile strength pattern was found similar to dry condition with visible reduction in the tensile strength of the scaffold in wet condition. In wet condition,

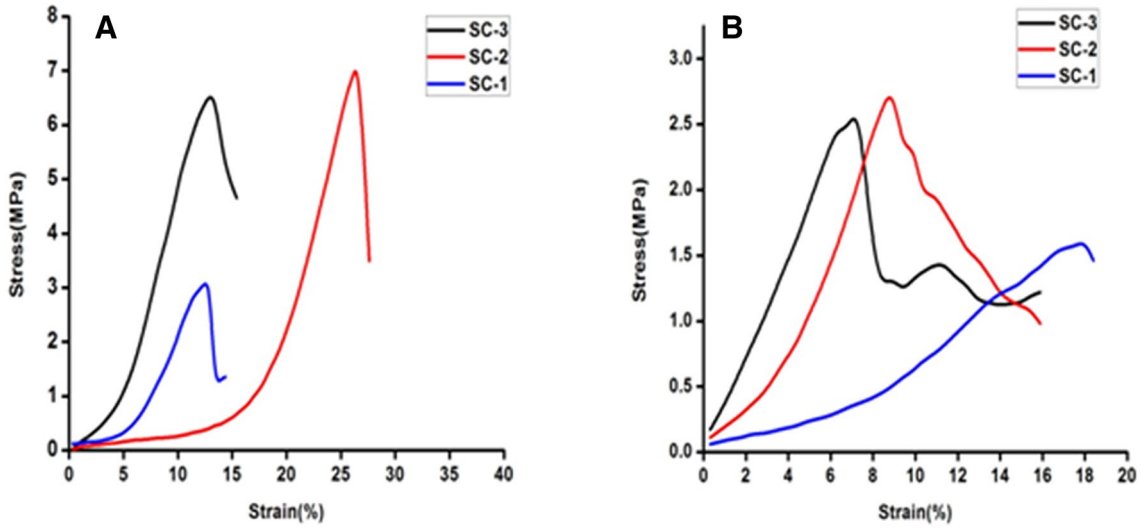

Fig. 4 **a** and **b** representing the mechanical strength of developed scaffolds under dry and wet condition, respectively

the tensile strength of scaffolds was found to be 1.58 MPa, 2.4 MPa and 2.62 MPa, respectively. Moreover, collagen has poor mechanical strength, therefore, it was mixed with chitosan to improvise the mechanical strength behavior in wet condition. Chitosan has inherent property of enhancing the mechanical strength with increasing concentration however it makes the scaffold brittle in nature. Chitosan helps to stabilize the open triple helix structure through hydrogen bonding. In Fig. 4a, SC-3 has depicted high tensile strength but low elasticity, whereas SC-1 shows low mechanical strength due to the less amount of the chitosan. SC-2 shows optimum tensile and strain bearing capacity compared to SC-1 and SC-3. In wet condition, scaffold absorbs water and get swelled due to which the tensile strength of scaffold get reduced and brittleness of SC-3 also gets compromised. Thus, appropriate blending of chitosan and collagen might be suitable to fabricate natural biopolymer-based scaffold with improvised mechanical properties for skin tissue engineering applications (Fig. 4).

Thermal property study

The weight loss in the scaffold samples occurred at various stages, the first one refers to the loss of water molecule associated with the scaffold at 25–200 °C followed by thermal degradation of the polymers at 200–400 °C and carbonization of material (400–700 °C) (Horn et al. 2009). Moreover, the obtained thermal graph showed the direct relationship between chitosan concentration and water loss. As the percentage of chitosan increases the percentage loss of water was also increased. Thus, it can be concluded that at the initial heating phase (25–200 °C) SC-2 and SC-3 showed high loss of structural water molecules as compare to SC-1. Hence, thermal degradation was observed less in SC-2 and SC-3 compared to SC-1. This might be due to interaction of collagen and chitosan that resulted into stabilization of collagen triple helical peptide structure and higher chitosan proportion in the blend might added the thermal stability of SC-2 and SC-3 (Fernandes et al. 2011). Thereby, scaffolds were stable up to 200 °C without any kind of alteration or change in its chemical and physical properties hence it can be efficiently used for the tissue engineering (Fig. 5, Table 2).

DSC pattern of scaffold was depicted in (Fig. 5b). The characteristic endothermic peaks represent the temperature of dehydration (T_D) of individual scaffold in the presence of nitrogen gas. The T_D values along with the enthalpy of dehydration (ΔH_D) are listed in Table 3. These DSC results clearly indicates T_D value of scaffold which increases with increasing chitosan concentration and this might be due to

Table 2 Representing the thermal degradation of scaffolds with temperature

	Peak maximum temperature (°C)	Percentage of weight loss		
		35–200 °C	200–400 °C	500–700 °C
Scaffold-1	373.6	8.9	35.56	8.65
Scaffold-2	303.7	5.35	40.26	16.20
Scaffold-3	286.9	3.62	47.45	6.65

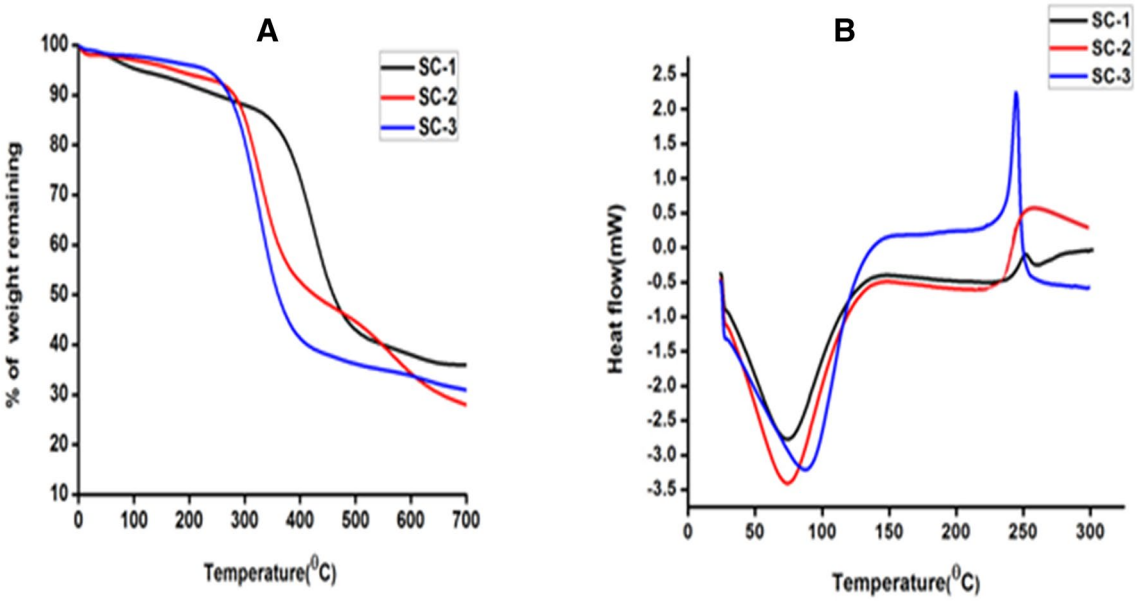

Fig. 5 Thermal behavior of developed scaffolds. **a** Representing TGA curve showing the percentage of weight loss with temperature. **b** Showing DSC pattern of scaffolds representing the endothermic peaks

Table 3 Depicting the thermal properties of scaffolds (T_D temperature of dehydration, ΔH_D enthalpy of dehydration)

Scaffold	SC-1	SC-2	SC-3
T_D (°C)	74	76	96
ΔH_D (J/g)	272	332	352

the stabilization of the collagen super coiled structure when comes in contact with chitosan. This was perfectly coordinated with the increase in the ΔH_D of the scaffold. Moreover, increases in the ΔH_D show consistency with the greater stabilization of the intermolecular interaction between the collagen and chitosan molecule.

Antimicrobial study

The antibacterial effect of selected scaffold (SC-2) was examined against the two types of bacteria that usually involved in wound infections, i.e., *E. coli* (Gram negative) and *S. aureus* (Gram positive). Control samples shows no zone of inhibition and thus shows poor antimicrobial activity against any of the two bacteria, while antibiotic-loaded scaffold has a clear zone of inhibition in agar plate against both the bacteria. Zone of inhibition produced in both agar plates was about 20 ± 1.8 mm and 18 ± 1.4 mm in diameter against *E. coli* and *S. aureus*, respectively. Hence, scaffold has antibacterial properties which can be used for wound healing applications to prevent bacterial infection and promote tissue regeneration (Fig. 6).

Haemocompatibility study

Haemocompatibility test was performed to evaluate the percentage of erythrocytes broken or ruptured when scafold comes in contact with blood. Evaluation of haemocompatibility is necessary before proceeding for any in vivo study. Our result showed the percent haemolysis (%) of scaffold was found to be 1.25, 1.32 and 1.42 for SC-1, SC-2 and SC-3, respectively. Haemolysis percentage was found to be less than 5% which clearly indicates the higher degree of haemocompatibility that make it suitable for further for in vivo study.

In vitro drug release

Release pattern of ciprofloxacin with time

One of the objectives of our study was to fabricate ciprofloxacin-loaded collagen–chitosan scaffold that can release antibiotic to provide the necessary protection against any kind of bacterial infections. There are many factors that affect the drug release including water solubility, permeability, and degree of crystallinity of antibiotic. In addition, nature of polymer (hydrophilicity and hydrophobicity) used for the fabrication of scaffold, method of scaffold preparation and cross-linking, nature of cross-linker are other parameters that affect the drug release (Fig. 7).

For active wound healing management, suitable and appropriate release properties of the antibiotics must be taken in account, which depend heavily on type of wound and the antibiotics. Based on type of wound such as fresh wound which need burst or quick release of antibiotic, whereas epithelialized wound need stable release of antibiotics (Leung et al. 2011).

Such rapid antibiotic release in initial 4–6 h followed by stable antibiotic release is desirable especially in early stage of wound healing (inflammation stage). It has been reported that collagen and chitosan-based hydrogels shows rapid release of antibiotics while employed for wound healing (Mahmoud and Salama 2016; Amiel et al. 2020; Arafat et al. 2019; Suhaeri et al. 2018; Ioan et al. 2020). Thus, the developed matrix designed specifically for active wound

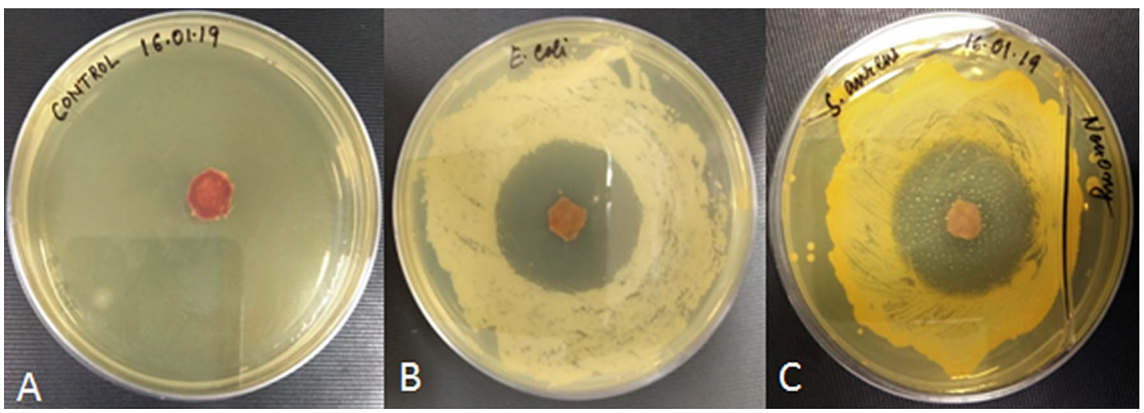

Fig. 6 Antibacterial effect of scaffold **a** Control **b** Against the growth of Gram-negative bacteria *E. coli*. **c** Against the growth of Gram-positive bacteria *S. aureus*

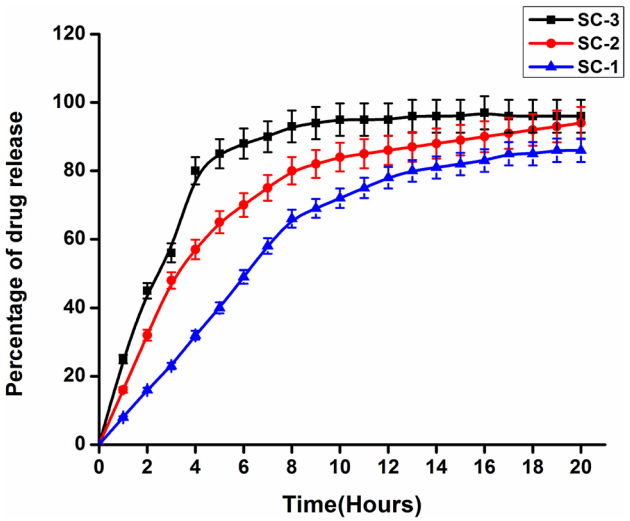

Fig. 7 Time-dependent release pattern of ciprofloxacin from the developed scaffolds

need to prevent infection thereby rapid drug releasing scaffold was designed.

In present study, freeze drying method was used for the scaffold preparation which provides highly porous structure. This high porosity provides high surface to volume ratio that leads to the rapid and high release of drug ciprofloxacin. The high drug release efficiency varied from 78 to 94% as depicted in Fig. 7. Such rapid release of antibiotic is desirable as it provides protection against microbes that may infect the wound form the surrounding.

SC-1 initially showed slow and sustained release, while SC-2 and SC-3 showed the rapid release of antibiotic. This difference is due to the change in the architecture of scaffold after coming in contact with PBS. SC-1 has high collagen content that makes it mechanically unstable and it also forms gel like structure that reduces its surface to volume ratio, therefore, reduces its drug release efficiency. SC-3 is mechanically stable and has high swelling percentage that has lead to the enhancement in surface to volume ratio which leads to the rapid release. SC-2 has maintained the structural integrity and has optimum and intermediate swelling percentage, therefore, shows rapid release in initial phase and sustained and continuous release in later phase.

Cell attachment and cell proliferation study

Cellular biocompatibility of developed COL/CHI/CPX scaffolds was investigated in vitro by evaluating the attachment, spreading, proliferation, and migration of fibroblast over the scaffolds. Cell attachment, proliferation and migration over the scaffold are the essential features of scaffold to support, promote and facilitate the function of wound healing. SEM images of cell seeded scaffold shown in Fig. 8 have clear indication that fibroblast cells were attached over the surface of all the scaffolds and started to proliferate. It has been also shown that scaffold after 10 and 15 days form monolayer like structure where cells were interconnected and attached over the scaffolds. Cultured scaffolds (SC-1, SC-2 and SC-3) stained with DAPI are shown in Fig. 9 for the duration of 5, 10 and 15 days, respectively. Fluorescent image revealed the successive increase in the cell number over the scaffolds with time. It was observed that SC-2 showed better cell growth as compare to rest that also been further supported by the SEM image of the mentioned scaffold. This might be due to suitable scaffold architecture, mechanical properties and swelling behavior of SC-2 as compared to SC-3 which has very high swelling percentage that leads to destabilization of scaffold architecture. All these factors make SC-2 more suitable than rest for cell attachment, growth, and proliferation (Figs. 8 and 9).

DNA content estimation

Cell proliferation on the scaffolds was quantified through estimation of total DNA content. The amount of DNA was quantified after 5 days and was found to be 1805.24 ± 0.54 ng/scaffold, 2089.21 ± 0.47 ng/scaffold and 2214.52 ± 0.84 ng/scaffold for SC-1, SC-2, and SC-3, respectively. After day 5, the cell number increases and the DNA content double (Fig. 10). After 10 days, the cells proliferate and DNA content was found to be 3589.25 ± 0.52 ng/scaffold, 4710.78 ± 0.85 ng/scaffold and 4187.87 ± 0.24 ng/scaffold for SC-1, SC-2, and SC-3, respectively. After 10 days, the cell has migrated throughout scaffold and the process of cell division tends to slowdown. Thereby, observed DNA content on day 15 was 5545.52 ± 28, 7432.54 ± 57 and 6546.87 ± 0.54 ng/scaffold for SC-1, SC-2 and SC-3, respectively. Moreover, chitosan in high concentration swells more than in low concentration and ultimately leads to higher porosity and larger pore size due to which cellular growth was higher in scaffold 2 and 3 in comparison to the scaffold 1. While SC-2 showed higher growth in comparison to the SC-3, because it swells and degrades faster in comparison to the SC-2 (Fig. 10).

MTT assay

The result of MTT assay showed that the metabolic activity of SC-2 was higher comparison to other scaffolds, which might be due to suitable pore size, mechanical integrity and optimum swelling of SC-2. Previous studies have reported that the structural integrity of the scaffold is necessary for the cellular growth and migration. Also, pore size of scaffold in between 80 and 150 µm was reported to be suitable for fibroblast growth over the porous scaffold (Fig. 11).

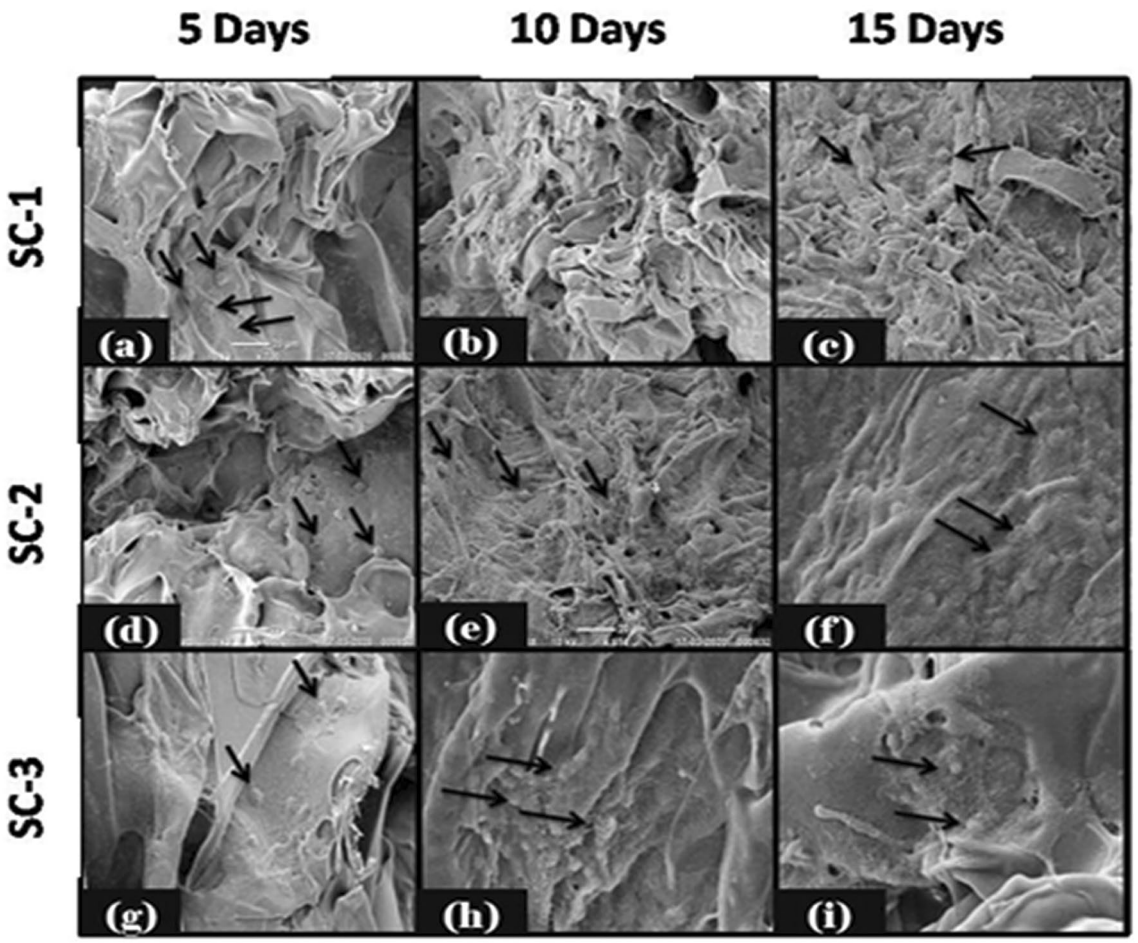

Fig. 8 SEM images of cell seeded scaffolds depicting the attachment of fibroblast after 5th, 10th, and 15th day. SC-2 showed more compatibility than rest for the attachment, growth, and proliferation of fibroblast

SC-1 has pore size of ~ 71 µm which was in lower range that makes it less suitable for the growth of fibroblast compare to the other set of scaffolds. As previously discussed, mechanical integrity of SC-1 get compromised in wet condition, which may lead to collapse of pore architecture during cell culture that may have resulted in low cell proliferation and low cell migration.

Besides SC-2, SC-3 also showed better growth of fibroblast over the scaffolds, which might be due to suitable mechanical strength and development of better pore architecture to support cell attachment and growth. Many studies have shown that scaffold with good mechanical strength and higher pore connectivity shows higher rate of cell growth, cell migration, and proliferation (Jithendra et al. 2013).

However, SC-3 has greater degree of porosity compared to SC-2. Very high porosity is not suitable for cell growth, because it may damage the internal architecture of scaffold that ultimately leads to the adverse affects in cell growth and migration (Fig. 11).

In vivo studies

During the in vivo study, wound healing rate in control and test group was compared at different time intervals. Images of wound were captured at 5th, 10th, and 15th day and the surface area was calculated to evaluate the rate of wound healing and closure (Fig. 12a), image representing the wound healing with time, (Fig. 12b and c) showing rate of wound closure and wound healing, respectively. On day 0, the wound having area of 225 mm^2 was treated with SC-2 and control was devoid of scaffold. On day 5, healing was observed with reduction in wound area from 225 mm^2 to 164 ± 7.2 mm^2 and 130 ± 4 mm^2, which shows $27 \pm 2.5\%$ and $42 \pm 2.7\%$ of wound healing in control and scaffold treated groups, respectively. After day 5, the rate of wound healing accelerated and on 10th day area of wound remained 103 ± 4.5 mm^2 and 63 ± 0.45 mm^2 that represents 54.15% and 72.5% of wound healing in control and scaffold treated groups, respectively. On 15th day, scaffold treated wound showed complete recovery while control group showed

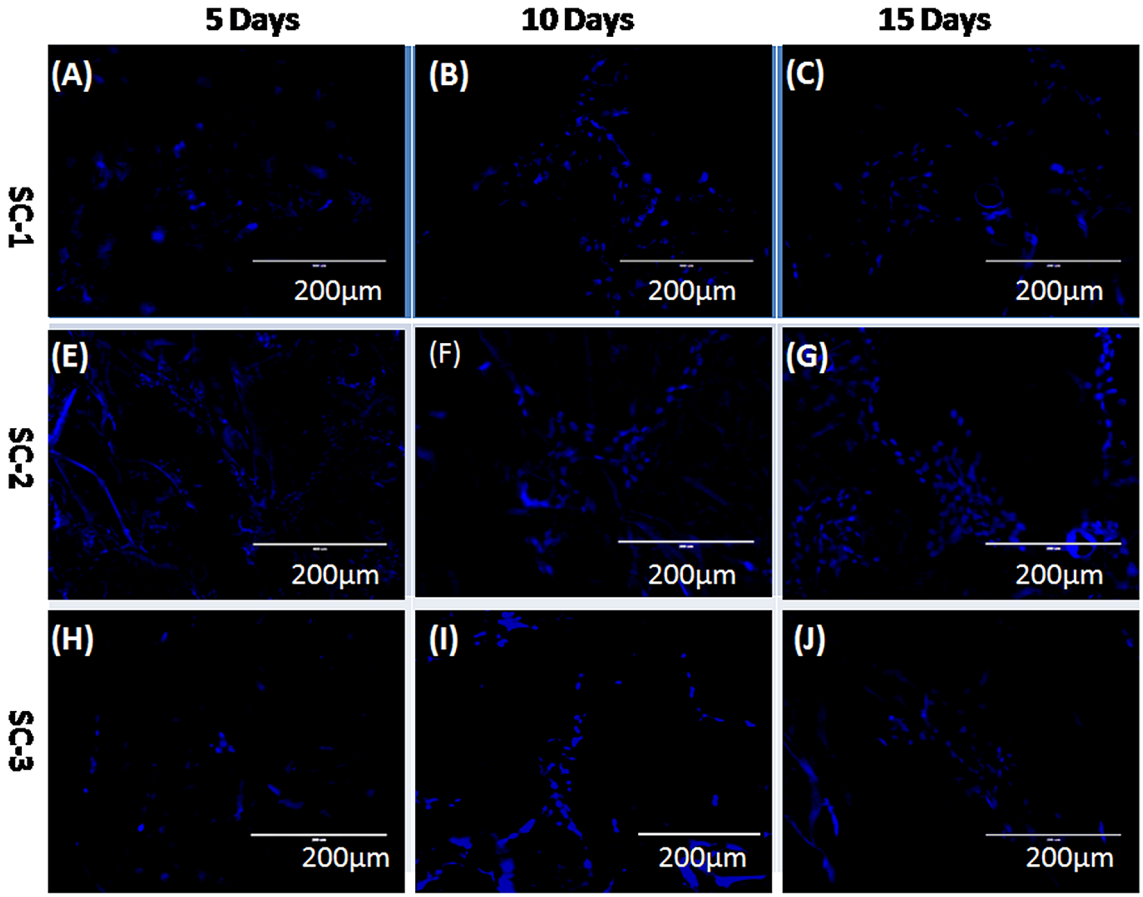

Fig. 9 Fluorescence microscopy images of cell seeded scaffolds stained with DAPI showing the growth and proliferation of fibroblast after 5th, 10th, and 15th day

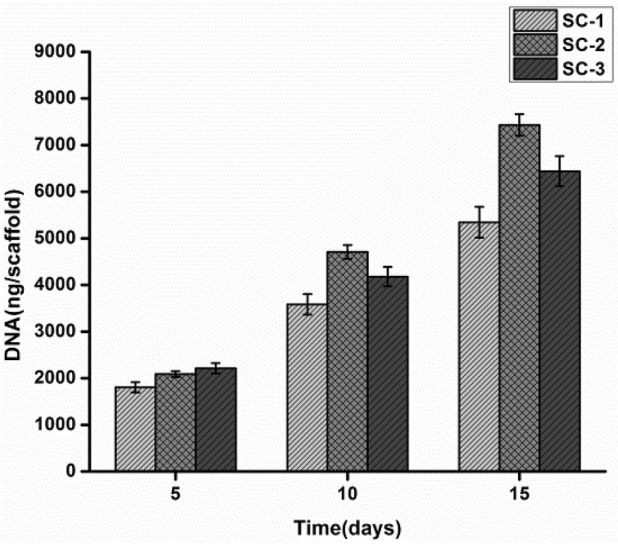

Fig. 10 Total DNA content of fibroblast present inside the scaffold was quantified at different time intervals

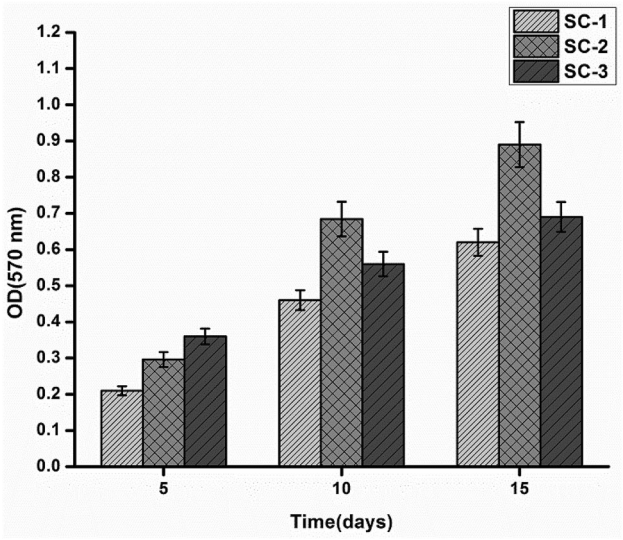

Fig. 11 Time-dependent effect of developed scaffolds on proliferation and viability of fibroblast

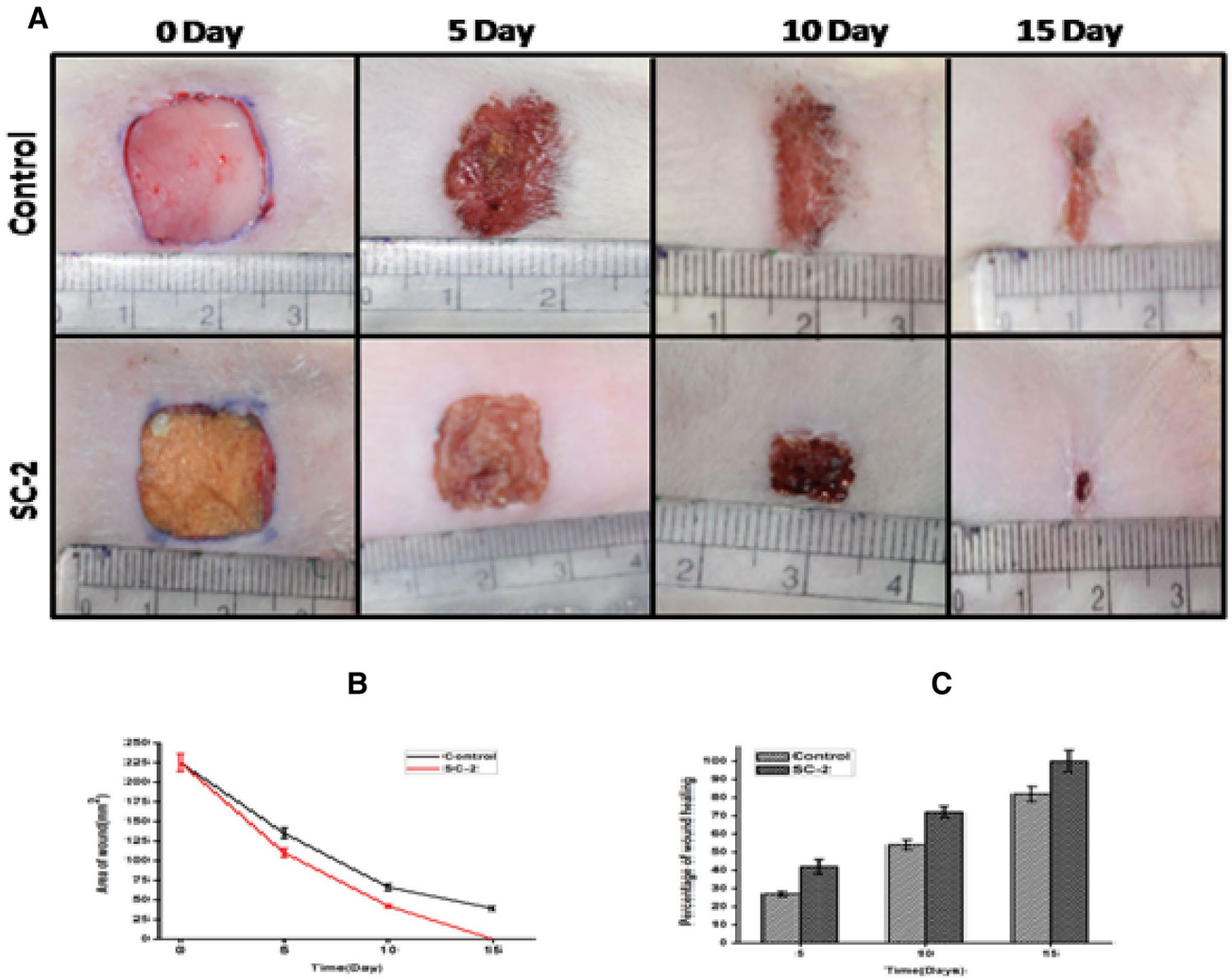

Fig. 12 **a** Representing wound healing potency of control and SC-2-treated groups at different time intervals and images were captured at 0, 5th, 10th and 15th day. **b** Representing rate of wound closure. **c** Representing the rate of wound heling

82.25% wound healing. There are two main factors which escalated the rate of healing and recovery. One is the utilization of collagen and chitosan in the process of wound healing and second is the Ciprofloxacin, an antibiotic in the scaffold that protected the wound against the bacterial infection and inflammation thus helped to accelerate the process of healing (Fig. 12).

Histological study

Histological stuies were performed using Hematoxylin and Eosin staining on 5th, 10th, and 15th day of wound healing in test and control groups. Microscopic studies revealed the macroscopic appearances along with some differences in the quality of wound healing. Process of epidermis and dermis formation was observed to be slowed in control as compared to scaffold treated wound which showed well-developed and thick dermis compared to control (Fig. 13). Architecture of connective tissues below the dermis is irregular and haphazard in control. Scaffold-treated wound shows better differentiation into outer and inner zones, which is the result of better remodeling of extracellular matrix compare to control. Besides, all these differences well organized granulation was seen at the latter stage of healing in scaffold compare to control that lacks organized granulation (Fig. 13).

Conclusion

In conclusion, we have illustrated the role of ciprofloxacin-loaded collage–chitosan scaffold for skin tissue engineering applications. Herein, we have discussed the fabrication and optimization of COL/CHI/CPX scaffold using freeze drying method. To maintain the architecture

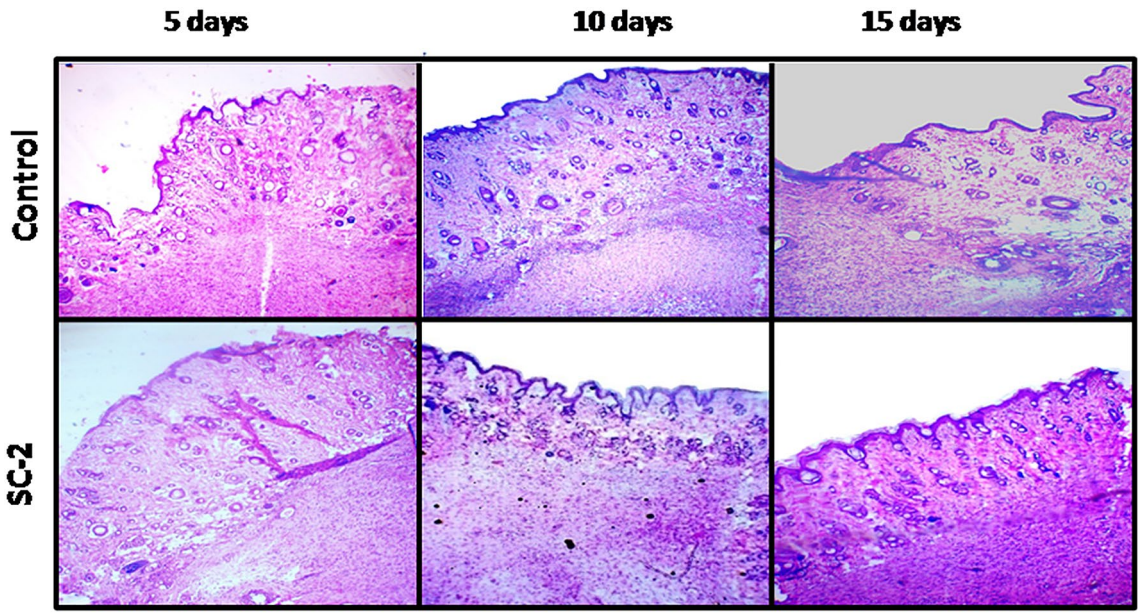

Fig. 13 Histological examination of control and SC-2-treated groups at different time intervals and images were captured at 0, 5th, 10th and 15th day at 10 × magnification

and integrity of scaffold EDC–NHC and glutaraldehyde was used for dual cross-linking. Proportion of collagen and chitosan has shown a vital role in determination of pore structure, architecture, swelling, degradation, and mechanical properties of scaffolds. Developed scaffold has shown excellent hemocompatibility and cell attachment, proliferation, growth, and migration of fibroblast on scaffolds. Developed scaffolds have antibacterial effect against most common wound growing bacterium such as *E.coli* and *S. aureus*. Furthermore, apart from in vitro studies, in vivo studies were also performed for the evaluation of COL/CHI/CPX scaffold. Histological studies have confirmed the better wound healing potential of developed scaffold thus might be a suitable biomaterial for skin tissue regeneration.

Acknowledgements This study was supported by the Central Instrument Facility Center (CIFC) and Ministry of Human Resource Development (MHRD), India.

Author contribution ST designed and performed the experiments and co-wrote the manuscript. BNS and DS characterized scaffold and co-wrote the manuscript. GK performed the histology study. PS conceived and supervised the complete study.

Compliance with ethical standards

Conflict of interest The authors declare that there is no conflict of interest in the publication.

Ethical statements The animal study were performed as per the protocol for animal use and approved by the Central Animal Ethical Committee at Institute of Medical Sciences, Banaras Hindu University, Varanasi (Registration no. DEAN/2017/CAEA/99).

References

Ahmadi F, Oveisi Z, Samani SM, Amoozgar Z (2015) Chitosan based hydrogels: characteristics and pharmaceutical applications. Res Pharm Sci 10(1):1

Amiel AG, Palomino-Durand C, Maton M, Lopez M, Cazaux F, Chai F, Neut C, Foligné B, Martel B, Blanchemain N (2020) Designed sponges based on chitosan and cyclodextrin polymer for a local release of ciprofloxacin in diabetic foot infections. Int J Pharm 587:119677

Andonegi M, Irastorza A, Izeta A, Cabezudo S, de la Caba K, Guerrero P (2020) A green approach towards native collagen scaffolds: environmental and physicochemical assessment. Polymers 12(7):1597

Arafat MT, Tronci G, Wood DJ, Russell SJ (2019) In-situ crosslinked wet spun collagen triple helices with nanoscale-regulated ciprofloxacin release capability. Mater Lett 255:126550

Arakawa C, Ng R, Tan S, Kim S, Wu B, Lee M (2017) Photopolymerizable chitosan–collagen hydrogels for bone tissue engineering. J Tissue Eng Regen Med 11(1):164–174

Boucard N, Viton C, Agay D, Mari E, Roger T, Chancerelle Y, Domard A (2007) The use of physical hydrogels of chitosan for skin regeneration following third-degree burns. Biomaterials 28(24):3478–3488

Chajra H, Rousseau C, Cortial D, Ronziere M, Herbage D, Mallein-Gerin F, Freyria A (2008) Collagen-based biomaterials and cartilage engineering. Application to osteochondral defects. Biomed Mater Eng 18(s1):33–45

Chen H, Xing X, Tan H, Jia Y, Zhou T, Chen Y, Ling Z, Hu X (2017) Covalently antibacterial alginate–chitosan hydrogel dressing

integrated gelatin microspheres containing tetracycline hydrochloride for wound healing. Mater Sci Eng C 70:287–295
Chhabra P, Tyagi P, Bhatnagar A, Mittal G, Kumar A (2016) Optimization, characterization, and efficacy evaluation of 2% chitosan scaffold for tissue engineering and wound healing. J Pharm Bioallied Sci 8(4):300
Chong EJ, Phan TT, Lim IJ, Zhang Y, Bay BH, Ramakrishna S, Lim CT (2007) Evaluation of electrospun PCL/gelatin nanofibrous scaffold for wound healing and layered dermal reconstitution. Acta Biomater 3(3):321–330
Dey S, Pal S (2009) Evaluation of collagen-hydroxyapatite scaffold for bone tissue engineering. In: 13th International conference on biomedical engineering. Springer, pp. 1267–1270
Dong C, Lv Y (2016) Application of collagen scaffold in tissue engineering: recent advances and new perspectives. Polymers 8(2):42
Enoch S, Leaper DJ (2008) Basic science of wound healing. Surgery (Oxford) 26(2):31–37
Fernandes LL, Resende CX, Tavares DS, Soares GA, Castro LO, Granjeiro JM (2011) Cytocompatibility of chitosan and collagen-chitosan scaffolds for tissue engineering. Polímeros 21(1):1–6
Francesko A, Tzanov T (2010) Chitin, chitosan and derivatives for wound healing and tissue engineering. Biofunctionalization of polymers and their applications. Springer, Berlin, Heidelberg, pp 1–27
Heo DN, Yang DH, Lee JB, Bae MS, Kim JH, Moon SH, Chun HJ, Kim CH, Lim H-N, Kwon IK (2013) Burn-wound healing effect of gelatin/polyurethane nanofiber scaffold containing silver-sulfadiazine. J Biomed Nanotechnol 9(3):511–515
Hollister SJ (2005) Porous scaffold design for tissue engineering. Nat Mater 4(7):518–524
Hopkinson I (1992a) Growth factors and extracellular matrix biosynthesis. J Wound Care 1(2):47–50
Hopkinson I (1992b) Molecular components of the extracellular matrix. J Wound Care 1(1):52–54
Horn MM, Martins VCA, de Guzzi Plepis AM (2009) Interaction of anionic collagen with chitosan: effect on thermal and morphological characteristics. Carbohydr Polym 77(2):239–243
Intini C, Elviri L, Cabral J, Mros S, Bergonzi C, Bianchera A, Flammini L, Govoni P, Barocelli E, Bettini R (2018) 3D-printed chitosan-based scaffolds: an in vitro study of human skin cell growth and an in-vivo wound healing evaluation in experimental diabetes in rats. Carbohydr Polym 199:593–602
Ioan D-C, Rău I, Albu Kaya MG, Radu N, Bostan M, Zgârian RG, Tihan GT, Dinu-Pîrvu C-E, Lupuliasa A, Ghica MV (2020) Ciprofloxacin-collagen-based materials with potential oral surgical applications. Polymers 12(9):1915
Jayakumar R, Prabaharan M, Kumar PS, Nair S, Tamura H (2011) Biomaterials based on chitin and chitosan in wound dressing applications. Biotechnol Adv 29(3):322–337
Jia Y, Hu Y, Zhu Y, Che L, Shen Q, Zhang J, Li X (2011) Oligoamines conjugated chitosan derivatives: Synthesis, characterization, in vitro and in vivo biocompatibility evaluations. Carbohydr Polym 83(3):1153–1161
Jin G, Prabhakaran MP, Ramakrishna S (2011) Stem cell differentiation to epidermal lineages on electrospun nanofibrous substrates for skin tissue engineering. Acta Biomater 7(8):3113–3122
Jithendra P, Rajam AM, Kalaivani T, Mandal AB, Rose C (2013) Preparation and characterization of aloe vera blended collagen-chitosan composite scaffold for tissue engineering applications. ACS Appl Mater Interfaces 5(15):7291–7298
Karri VVSR, Kuppusamy G, Talluri SV, Mannemala SS, Kollipara R, Wadhwani AD, Mulukutla S, Raju KRS, Malayandi R (2016) Curcumin loaded chitosan nanoparticles impregnated into collagen-alginate scaffolds for diabetic wound healing. Int J Biol Macromol 93:1519–1529
Khandelwal G, Minocha T, Yadav SK, Chandrasekhar A, Raj NPMJ, Gupta SC, Kim S-J (2019) All edible materials derived biocompatible and biodegradable triboelectric nanogenerator. Nano Energy 65:104016
Kim SE, Heo DN, Lee JB, Kim JR, Park SH, Jeon SH, Kwon IK (2009) Electrospun gelatin/polyurethane blended nanofibers for wound healing. Biomed Mater 4(4):044106
Kim S, Cui Z-K, Koo B, Zheng J, Aghaloo T, Lee M (2018) Chitosan-lysozyme conjugates for enzyme-triggered hydrogel degradation in tissue engineering applications. ACS Appl Mater Interfaces 10(48):41138–41145
Kumari S, Singh BN, Srivastava P (2019) Effect of copper nanoparticles on physico-chemical properties of chitosan and gelatin-based scaffold developed for skin tissue engineering application. 3 Biotech 9(3):102
Kumbar SG, Nukavarapu SP, James R, Nair LS, Laurencin CT (2008) Electrospun poly (lactic acid-co-glycolic acid) scaffolds for skin tissue engineering. Biomaterials 29(30):4100–4107
Leung V, Hartwell R, Yang H, Ghahary A, Ko F (2011) Bioactive nanofibres for wound healing applications. J Fiber Bioeng Inf 4(1):1–14
Lim MM, Sultana N (2016) In vitro cytotoxicity and antibacterial activity of silver-coated electrospun polycaprolactone/gelatine nanofibrous scaffolds. 3 Biotech 6(2):211
Liu T, Dan W, Dan N, Liu X, Liu X, Peng X (2017) A novel grapheme oxide-modified collagen-chitosan bio-film for controlled growth factor release in wound healing applications. Mater Sci Eng C 77:202–211
Loh QL, Choong C (2013) Three-dimensional scaffolds for tissue engineering applications: role of porosity and pore size. Tissue Eng Part B Rev 19(6):485–502
Ma L, Gao C, Mao Z, Zhou J, Shen J, Hu X, Han C (2003) Collagen/chitosan porous scaffolds with improved biostability for skin tissue engineering. Biomaterials 24(26):4833–4841
Mabrouk M, Mostafa A, Oudadesse H, Mahmoud AA, El-Gohary MI (2014) Effect of ciprofloxacin incorporation in PVA and PVA bioactive glass composite scaffolds. Ceram Int 40(3):4833–4845
Mahato KK, Yadav I, Singh R, Singh BN, Singh SK, Ray B, Kumar M, Misra N (2019) Polyvinyl alcohol/chitosan lactate composite hydrogel for controlled drug delivery. Mater Res Express 6(11):115408
Mahmoud AA, Salama AH (2016) Norfloxacin-loaded collagen/chitosan scaffolds for skin reconstruction: preparation, evaluation and in-vivo wound healing assessment. Eur J Pharm Sci 83:155–165
Mallick SP, Singh BN, Rastogi A, Srivastava P (2018) Design and evaluation of chitosan/poly (L-lactide)/pectin based composite scaffolds for cartilage tissue regeneration. Int J Biol Macromol 112:909–920
Maquet V, Boccaccini AR, Pravata L, Notingher I, Jérôme R (2004) Porous poly (α-hydroxyacid)/Bioglass® composite scaffolds for bone tissue engineering. I: preparation and in vitro characterisation. Biomaterials 25(18):4185–4194
Mayet N, Choonara YE, Kumar P, Tomar LK, Tyagi C, Du Toit LC, Pillay V (2014) A comprehensive review of advanced biopolymeric wound healing systems. J Pharm Sci 103(8):2211–2230
Metcalfe AD, Ferguson MW (2007) Tissue engineering of replacement skin: the crossroads of biomaterials, wound healing, embryonic development, stem cells and regeneration. J R Soc Interface 4(14):413–437
Mitra S, Ghosh N, Banerjee E (2018) Carboxymethyl Guar Gum nanoscaffold as matrix for cell growth. Vitro
Nguyen TTT, Ghosh C, Hwang S-G, Dai Tran L, Park JS (2013) Characteristics of curcumin-loaded poly (lactic acid) nanofibers for wound healing. J Mater Sci 48(20):7125–7133
Sa G, DiPietro LA (2010) Factors affecting wound healing. J Dent Res 89(3):219–229

Seluanov A, Vaidya A, Gorbunova V (2010) Establishing primary adult fibroblast cultures from rodents. J Vis Exp 44:e2033

Shah R, Stodulka P, Skopalova K, Saha P (2019) Dual crosslinked collagen/chitosan film for potential biomedical applications. Polymers 11(12):2094

Shevchenko RV, James SL, James SE (2010) A review of tissue-engineered skin bioconstructs available for skin reconstruction. J R Soc Interface 7(43):229–258

Singh B, Pramanik K (2018) Fabrication and evaluation of non-mulberry silk fibroin fiber reinforced chitosan based porous composite scaffold for cartilage tissue engineering. Tissue Cell 55:83–90

Singh BN, Veeresh V, Mallick SP, Sinha S, Rastogi A, Srivastava P (2020) Generation of scaffold incorporated with nanobioglass encapsulated in chitosan/chondroitin sulfate complex for bone tissue engineering. Int J Biol Macromol 153:1–16

Sionkowska A (2011) Current research on the blends of natural and synthetic polymers as new biomaterials. Prog Polym Sci 36(9):1254–1276

Sizeland KH, Hofman KA, Hallett IC, Martin DE, Potgieter J, Kirby NM, Hawley A, Mudie ST, Ryan TM, Haverkamp RG (2018) Nanostructure of electrospun collagen: do electrospun collagen fibers form native structures? Materialia 3:90–96

Suhaeri M, Noh MH, Moon J-H, Kim IG, Oh SJ, Ha SS, Lee JH, Park K (2018) Novel skin patch combining human fibroblast-derived matrix and ciprofloxacin for infected wound healing. Theranostics 8(18):5025

Sun K, Li H, Li R, Nian Z, Li D, Xu C (2015) Silk fibroin/collagen and silk fibroin/chitosan blended three-dimensional scaffolds for tissue engineering. Eur J Orthop Surg Traumatol 25(2):243–249

Susanto A, Susanah S, Priosoeryanto BP, Satari MH, Komara I (2019) The effect of the chitosan-collagen membrane on wound healing process in rat mandibular defect. J Indian Soc Periodontol 23(2):113

Suzuki Y, Nishimura Y, Tanihara M, Suzuki K, Nakamura T, Shimizu Y, Yamawaki Y, Kakimaru Y (1998) Evaluation of a novel alginate gel dressing: cytotoxicity to fibroblasts in vitro and foreign-body reaction in pig skin in vivo. J Biomed Mater Res 39(2):317–322

Tallian C, Tegl G, Quadlbauer L, Vielnascher R, Weinberger S, Cremers R, Pellis A, Salari JW, Guebitz GM (2019) Lysozyme-responsive spray-dried chitosan particles for early detection of wound infection. ACS Appl Bio Mater 2(3):1331–1339

Tangsadthakun C, Kanokpanont S, Sanchavanakit N, Banaprasert T, Damrongsakkul S (2017) Properties of collagen/chitosan scaffolds for skin tissue engineering. J Met Mater Miner 16 (1)

Torsteinsdóttir I, Håkansson L, Hällgren R, Gudbjörnsson B, Arvidson N-G, Venge P (1999) Serum lysozyme: a potential marker of monocyte/macrophage activity in rheumatoid arthritis. Rheumatology 38(12):1249–1254

Tylingo R, Gorczyca G, Mania S, Szweda P, Milewski S (2016) Preparation and characterization of porous scaffolds from chitosan–collagen–gelatin composite. React Funct Polym 103:131–140

Udhayakumar S, Shankar KG, Sowndarya S, Venkatesh S, Muralidharan C, Rose C (2017) l-Arginine intercedes bio-crosslinking of a collagen–chitosan 3D-hybrid scaffold for tissue engineering and regeneration: in silico, in vitro, and in vivo studies. RSC Adv 7(40):25070–25088

Ungureanu C, Ioniţă D, Berteanu E, Tcacenco L, Zuav A, Demetrescu I (2015) Improving natural biopolymeric membranes based on chitosan and collagen for biomedical applications introducing silver. J Braz Chem Soc 26(3):458–465

Unnithan AR, Barakat NA, Pichiah PT, Gnanasekaran G, Nirmala R, Cha Y-S, Jung C-H, El-Newehy M, Kim HY (2012) Wound-dressing materials with antibacterial activity from electrospun polyurethane–dextran nanofiber mats containing ciprofloxacin HCl. Carbohydr Polym 90(4):1786–1793

Venugopal J, Ramakrishna S (2005) Biocompatible nanofiber matrices for the engineering of a dermal substitute for skin regeneration. Tissue Eng 11(5–6):847–854

Wang P-Y, Tsai W-B (2013) Modulation of the proliferation and matrix synthesis of chondrocytes by dynamic compression on genipin-crosslinked chitosan/collagen scaffolds. J Biomater Sci Polym Ed 24(5):507–519

Wong S-C, Baji A, Gent AN (2008) Effect of specimen thickness on fracture toughness and adhesive properties of hydroxyapatite-filled polycaprolactone. Compos A Appl Sci Manuf 39(4):579–587

Wu L, Lin L, Qin Y-X (2015) Enhancement of cell ingrowth, proliferation, and early differentiation in a three-dimensional silicon carbide scaffold using low-intensity pulsed ultrasound. Tissue Eng Part A 21(1–2):53–61

Yu H, Xu X, Chen X, Hao J, Jing X (2006) Medicated wound dressings based on poly (vinyl alcohol)/poly (N-vinyl pyrrolidone)/chitosan hydrogels. J Appl Polym Sci 101(4):2453–2463